A hydroclimatic model for the distribution of fire on Earth

Environmental Research Communications

PAPER

A hydroclimatic model for the distribution of fire on Earth

Matthias M Boer[1], **Víctor Resco De Dios**[2,3], **Elisa Z Stefaniak**[1] and **Ross A Bradstock**[4]

[1] Hawkesbury Institute for the Environment, Western Sydney University, Richmond, Australia
[2] School of Life Science and Engineering, Southwest University of Science and Technology, Mianyang, People's Republic of China
[3] Department of Crop and Forest Sciences-JRU CTFC-AGROTECNIO, Universitat de Lleida, E 25198 Lleida, Spain
[4] Centre for Environmental Risk Management of Bushfires, University of Wollongong, Wollongong, Australia

E-mail: m.boer@westernsydney.edu.au

OPEN ACCESS

RECEIVED
15 October 2020

REVISED
4 March 2021

ACCEPTED FOR PUBLICATION
4 March 2021

PUBLISHED
25 March 2021

Keywords: wildfire, fire regime, climatic water balance, aridity index, fuel type, fuel dryness

Supplementary material for this article is available online

Abstract

The distribution of fire on Earth has been monitored from space for several decades, yet the geography of global fire regimes has proven difficult to reproduce from interactions of climate, vegetation, terrain, land use and other human activities by empirical and process-based fire models. Here, we propose a simple, yet robust, model for the global distribution of fire potential based on fundamental biophysical constraints controlling fire activity in all biomes. In our 'top-down' approach we ignored the dynamics of individual fires and focus on capturing hydroclimatic constraints on the production and (seasonal) desiccation of fuels to predict the potential mean annual fractional burned area at 0.25° spatial resolution, here estimated by the 0.99 quantile of the observed mean annual fractional burned area ($F_{0.99}$) over the 1995-2016 period of the Global Fire Emissions Database (GFED4). We show that 80% of the global variation in $F_{0.99}$ can be explained from a combination of mean annual precipitation and potential evapotranspiration. The proposed hydroclimatic model reproduced observed 0.99 quantile fire activity levels equally well across all biomes and provided the first objective underpinning for the dichotomy of global fire regimes in two domains characterised by either fuel production limitations on fire or fuel dryness limitations on fire. A sharp transition between the two climate-fire domains was found to occur at a mean annual aridity index of 1.9 (1.94 $\pm$ 0.02). Our model provides a simple but comprehensive basis for predicting fire potential under current and future climates, as well as an overarching framework for estimating effects of human activity via ignition regimes and manipulation of vegetation.

1. Introduction

Satellite-based Earth observation is providing an increasingly accurate picture of global fire patterns [1–4]. The highest fire activity is observed in seasonally dry (sub-)tropical environments of South America, Africa and Australia, but fires occur with varying frequency, intensity and seasonality in almost all biomes on Earth [5]. The particular combinations of these fire characteristics, or fire regimes [6], are known to emerge from the combined influences of climate, vegetation, terrain and land use, but their global distribution has so far proven difficult to reproduce by mathematical models [7–9]. Most current land surface models (LSMs) and Dynamic Global Vegetation Models (DGVMs) have some capacity to simulate fire activity from basic environmental variables but predictions [8, 10] usually only agree with observations in some biomes (e.g. savannas of the Sub-Saharan Africa), while disagreeing in others (e.g. boreal forests of North-America). Humans add further complexity to global fire patterns by, amongst others, changing vegetation community composition, structure and flammability, active use of fire to clear land or reduce fire hazard, and fire suppression [11–14]. The limited ability of current models in predicting global fire patterns suggests that their fire modules fail to capture some aspects of the biophysics that control fire activity across different environments. Incomplete understanding of biophysical drivers and constraints that underlie current global fire patterns creates uncertainty in model

predictions of how fire regimes, fire-prone ecosystems and related biogeochemical cycles may respond to rising atmospheric [CO_2] and climate change [15].

Here, we go back to the fundamental biophysics of fire to formulate a simple, yet robust, model for the prediction of potential mean annual levels of fire activity across all global biomes. For this study we define fire activity in terms of the climatological mean annual fractional burned area, F, of the landscape or land area unit, ranging from 0 in long unburnt landscapes to 1 in landscapes that burn completely on an annual basis [2]. By predicting F we ignore the dynamics of individual fires, but this is appropriate in our view given the fact that most fires are orders of magnitude smaller e.g., [5, 16] than the typical grid size (e.g. $0.5^\circ \times 0.5^\circ$) of LSMs and DGVMs.

Building on Bradstock's [17] 'four-switch' concept we assume that four fundamental conditions need to be met for a landscape fire to occur: (i) there must be enough plant biomass (i.e. fuel) to carry a fire, (ii) the extant fuel must be dry enough to be ignitable, (iii) weather conditions need to be favourable (i.e. hot, dry and windy) for a fire to spread, and (iv) there must be an ignition. Bradstock [17] conceptualized these conditions as four 'switches' in a series circuit that need to be 'on' for a fire to occur. While any fire will require alignment of all four switches at some point in time, in the context of modelling global fire patterns we emphasize that the four switches operate at disparate time scales, with an associated hierarchy of conditional constraints on fire: (1) production of plant biomass and build-up of fuel loads occurs over months to years, (2) fuels dry out over weeks to months, and (3) fire weather varies over time scales of hours to days, while (4) ignitions are instantaneous events. Therefore, we hypothesize that the mean annual fractional burned area (F) can be predicted from long-term fuel production and fuel drying rates (i.e. switches 1–2), while information on fire weather and ignitions (i.e. switches 3–4) is only required when modelling the specific attributes of individual fires (e.g. size and burn pattern). The hierarchical organization of the four switches further implies that the mean annual fractional burned area predicted from long-term fuel production and fuel drying rates alone represents an upper limit of mean annual fire activity that is only reached when fire weather and ignition limitations are minimal.

To test the hypothesis that the upper quantiles of F can be predicted from long-term fuel production and drying rates we analysed global burned area data together with indices of fuel productivity and fuel dryness, both calculated from the climatic water balance [18]. Building on the methods developed in a previous study of Australian fire regimes [19], we propose a new global model that predicts the long term upper limit (i.e. the 0.99 quantile, [20]) of the mean annual fractional burned area, $F_{0.99}$, from two basic hydroclimatic variables: mean annual precipitation, P, and potential evapotranspiration, E_0. The model provides a framework to quantify the relative importance of either fuel productivity or fuel dryness constraints on $F_{0.99}$, which we hypothesized to vary with the global distribution of land cover types and corresponding fuel types. Consistent with the varying constraints hypothesis [21], in dryland environments with grassy fuels we expected $F_{0.99}$ to be primarily limited by fuel productivity constraints (i.e. increase with P), while in more mesic environments dominated by woody vegetation and litter fuels $F_{0.99}$ was expected to be limited primarily by fuel dryness constraints (i.e. increase with E_0). Other studies [22, 23], focusing on fire regimes in the western USA, have related climatic water balance terms to seasonal area burned and interpreted the strength and sign of correlations to infer predominance of fuel production or fuel dryness constraints on fire at Bailey [24] ecosection level. Abatzoglou *et al* [25] showed that interannual variation in global burned area was positively correlated with climatic indices of fuel aridity in forested ecoregions and with cumulative precipitation prior to the fire season in non-forested ecoregions. To our knowledge the present study is the first to develop a universal hydroclimatic model that explains both global variation in burned area as well as the dichotomy of global fire regimes in two domains of either fuel production or fuel dryness limitations on fire. Finally, we explored whether the global distribution of contemporary fire regime classes or 'pyromes' as classified by Archibald *et al* [5] on the basis of five fire regime metrics (i.e. fire return interval, maximum fire intensity, length of fire season, maximum fire size, mean annual area burned) was associated with the relative importance of fuel productivity or fuel dryness constraints on $F_{0.99}$.

2. Materials and methods

2.1. Modelling approach

In this study our aim was to predict the global distribution of potential mean annual fractional burned area ($F_{0.99}$) as a function of basic biophysical constraints on the production and dryness of fuel material. Following Boer *et al* [19], we assumed that both the production and drying of fuel material are essentially functions of the local water and energy budgets available for the production and desiccation of plant biomass. The long-term climatic water balance, calculated from mean annual P and E_0, captures these interactions of biologically available water and energy [18]. When calculated over long time scales ($\gg$years) and broad spatial scales ($\gg$km^2), changes in the soil water store and lateral water inputs can be assumed to be negligible so that the climatic water balance is reduced to: $P - Q - E = 0$, where Q is runoff/drainage losses and E is actual

evapotranspiration. Here, we assume that seasonal lags between climate and fuel conditions can be ignored when relating mean annual burned area to mean annual water balance. E is a reliable predictor of continental patterns of annual primary productivity at annual timescales [26, 27] and therefore a reasonable proxy for fuel production rates [28, 29]. Similarly, the potential for drying of fuel material can be assumed to be proportional to the atmospheric moisture demand ($\propto E_0$) that cannot be met by available water ($\propto E$), which is the climatic water deficit as defined by Stephenson [18], $D = E_0 - E$. For long timescales and large land areas, E can be predicted from P and E_0 using the semi-empirical Budyko curve [30–32], which provides a global model for the partitioning of mean annual precipitation in runoff and evapotranspiration as a function of climatic aridity:

$$E = P\sqrt{\frac{E_0}{P}\tanh\left(\frac{E_0}{P}\right)^{-1}\left[1 - \exp\left(-\frac{E_0}{P}\right)\right]} \tag{1}$$

where P, E_0 and E are mean annual precipitation, potential evapotranspiration and actual evapotranspiration, respectively, and $(\frac{E_0}{P})$ is the aridity index. The reader is referred to Wang *et al* [33] for a review on applications of the Budyko framework in hydrology and water balance modelling.

Recently, Boer *et al* [19] demonstrated that continental patterns of $F_{0.99}$ in Australia can be accurately predicted from mean annual E and D, which can be approximated from P and E_0. Since most global fire regime classes are represented in Australia [5, 34], we hypothesized that the global distribution of $F_{0.99}$ can also be modelled as a function of mean annual E and D. Here we present a new global $F_{0.99}$ model that consists of two flexible sigmoidal functions, $F_{0.99}(E)$ and $F_{0.99}(D)$, describing the increase in $F_{0.99}$ with mean annual actual evapotranspiration (E) and climatic water deficit (D), respectively:

$$F_{0.99}(E) = \left[1 + \frac{E_2 - E}{E_2 - E_1}\right]\left[\frac{E}{E_2}\right]^{\frac{E_2}{(E_2 - E_1)}}$$

with $0 < E \leqslant E_2$

$$F_{0.99}(E) = 1 \text{ for } E > E_2 \tag{2}$$

$$F_{0.99}(D) = \left[1 + \frac{D_2 - D}{D_2 - D_1}\right]\left[\frac{D}{D_2}\right]^{\frac{D_2}{(D_2 - D_1)}}$$

with $0 < D \leqslant D_2$

$$F_{0.99}(D) = 1 \text{ for } D > D_2 \tag{3}$$

$$F_{0.99}(E, D) = F_{\max} F_{0.99}(E) F_{0.99}(D) \tag{4}$$

where $F_{\max}$ is the global maximum of $F_{0.99}$, here set at 1. The shape of $F_{0.99}(E)$ and $F_{0.99}(D)$ is set by two parameters [35]: E_1 (or D_1) is the value at which $F_{0.99}$ increases most strongly with E (or D), and E_2 (or D_2) the value at which $F_{0.99}$ becomes irresponsive to further increase of E (or D). Since the two predictor variables, E and D, are not independent, the fitted E, D, $F_{0.99}$ response surface was mapped to (orthogonal) axes of P and E_0 before interpreting the shape of the response surface in terms of global variation in biophysical constraints on potential fire activity.

2.2. Data

2.2.1. Burned area

Global annual burned area data at $0.25^\circ \times 0.25^\circ$ spatial resolution for the period July 1995–June 2016 were obtained from the GFED4 database, which has been widely used in global fire modelling studies. For full details on the GFED4 database, including caveats and limitation, the reader is referred to Giglio *et al* [2]. The mean annual fractional burned area, F, was calculated by summing the burned areas within each grid cell for the entire observation period and dividing by the area of the grid cell and the duration of the observation period.

2.2.2. Climatic water balance

Gridded mean annual precipitation for 1950–2000, P, was obtained from WorldClim [36], while gridded mean annual potential evapotranspiration for 1960–1990, E_0, based on the Hargreaves method [37, 38], was obtained from the Global Aridity and Potential Evapotranspiration Data base at CGIAR-CSI (http://www.cgiar-csi.org/data/global-aridity-and-pet-database). Both climate layers have a spatial resolution of 30 arcseconds and were resampled to the $0.25^\circ \times 0.25^\circ$ grid of the GFED4 data base using bilinear interpolation. Mean annual actual evapotranspiration, E, was predicted from P and E_0 using the Budyko curve (equation (1)).

2.2.3. Landcover and fuel types

This study focused on areas of (semi-)natural vegetation. The corresponding vegetation mask was constructed from the Land Cover Type product (MCD12Q1_V51) of the Moderate Resolution Imaging Spectroradiometer (MODIS), which corresponds to the end of the burned area and climate observation period used for our model. We first resampled the MCD12Q1_V51 data layer to the 0.25° × 0.25° grid of the GFED4 data base, using nearest neighbour interpolation, and then reclassified grid cells of excluded land cover types (i.e. water, cropland, urban and built-up, cropland/natural vegetation mosaics, snow and ice, barren or sparsely vegetated) to missing values.

2.3. Data analyses

2.3.1. Model fitting and validation

Data analyses focused on the modelling of the global distribution of $F_{0.99}$ as a function of mean annual E and D (equations (2)–(4)) and on the interpretation of the model in terms of its consistency with current understanding of global fire patterns. Our complete data set consisted of estimates of mean annual F, P, E_0, and E for 193,476 grid cells covering the selected land cover types of the global land area, except Antarctica, at 0.25° × 0.25° spatial resolution. A randomly selected sample of 50% of the grid cells was used for model fitting, while the other 50% of the data was set aside for model validation. We used R [39] for all data analyses, in particular the 'raster' [40] and 'quantreg' packages [41].

Non-linear quantile regression was used to fit equation (4) to the 0.99 quantile of F as a function of mean annual E and D. To minimize bias in the model towards the most common global climates (e.g. desert or boreal climates), we used a simple bootstrap procedure of two steps: (i) the global E, D space was divided into 100 mm by 100 mm bins and all climate bins with a minimum of 100 grid cells identified (n = 145), (ii) a random sample (with replacement) of 100 grid cells was drawn from these bins, and (iii) equation (4) was fitted to the sample data. This procedure was run 1000 times to generate 1000 response surfaces from which a mean $F_{0.99}$ response surface was calculated [42].

Model predictions were validated against the 50% of the data that was not used for model fitting. To do so the validation data was binned into 100 mm × 100 mm wide E, D bins and the corresponding values of $F_{0.99}$ identified for all bins with a minimum of 50 observations (n = 191). Predicted values of $F_{0.99}$ were extracted from the modelled mean response surface for the same set of 191 E, D data pairs. Observed values of $F_{0.99}$ correspond to the 0.99 quantile value of F in each of the 191 100 mm × 100 mm E, D bins. The relationship between observed and predicted $F_{0.99}$ was evaluated by linear regression analysis. Deviations between observed and predicted $F_{0.99}$ were quantified using the mean difference (MD) and root mean squared difference (RMSD):

$$MD = \sum_{i=1}^{n} (\hat{y}_i - y_i)/n \tag{5}$$

$$RMSD = \sqrt{\sum_{i=1}^{n} (\hat{y}_i - y_i)^2/n} \tag{6}$$

where $\hat{y}_i$, y_i are predicted and observed values of $F_{0.99}$ and n = 191. To measure agreement between the spatial patterns of observed and predicted $F_{0.99}$, we used the normalised mean error (NME) and normalised mean squared error (NMSE), as proposed by Kelley *et al* [43]:

$$NME = \sum_i |\hat{y}_i - y_i| / \sum_i |y_i - \bar{y}| \tag{7}$$

$$NMSE = \sum_i (\hat{y}_i - y_i)^2 / \sum_i (y_i - \bar{y})^2 \tag{8}$$

where $\hat{y}_i$ is the predicted value of $F_{0.99}$ at grid cell i, y_i the corresponding observed value, and $\bar{y}$ the mean of all observed values. By normalising by the spatial variability of the observations, NME and NMSE provide a measure of the spatial error of the model, with NME or NMSE close to 0 indicating perfect agreement between observed and predicted patterns, and both metrics approaching unity when agreement is similar to that of a model that predicts a spatially uniform value equal to the mean of all observations [43].

2.3.2. Identification of climate-fire domains

Following Boer *et al* [19] two climate-fire domains were distinguished on the P, E_0, $F_{0.99}$ response surface depending on whether the direction of the $F_{0.99}$ gradient was more parallel to the local E gradient or D gradient, indicating predominance of fuel productivity or fuel dryness limitation on fractional burned area, respectively. The boundary between the two climate-fire domains was identified analytically using a gradient analysis of the $F_{0.99}$ response surface relative to gradients of E and D in P, E_0 space (Supplementary Material, S3).

As in Boer *et al* [19] we refer to these two domains as productivity-limited (PL) fire and dryness-limited (DL) fire domains and analysed whether the affinity to either domain was related to the vegetation type being

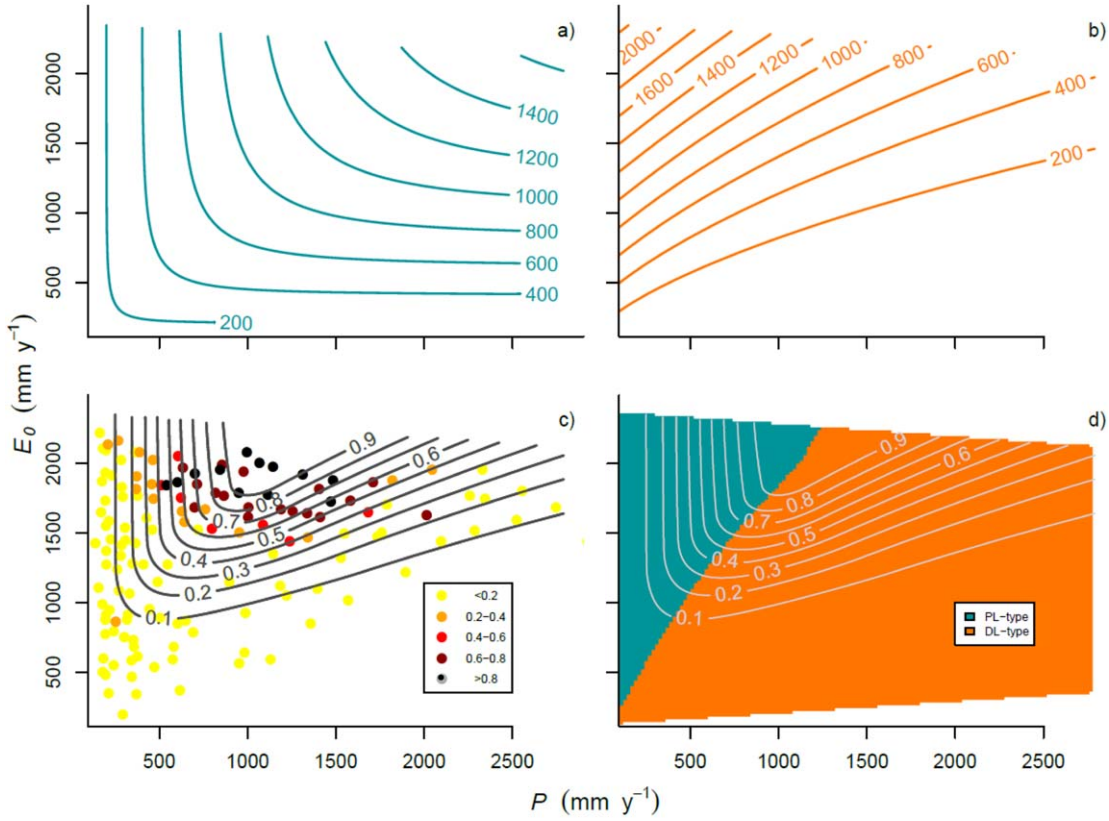

Figure 1. (a) Mean annual actual evapotranspiration (E, mm.y^{-1}), (b) climatic water deficit (D, mm.y^{-1}), and (c) the 0.99 quantile of mean annual fractional burned area ($F_{0.99}$) as functions of mean annual precipitation (P) and potential evapotranspiration (E_0). (d) Distribution of the domains of PL- and DL-type fire in P, E_0 space, with contours of the $F_{0.99}$ model in grey. Coloured dots in panel (c) correspond to independent observations of $F_{0.99}$ used for validation.

dominated by grasses/herbaceous or woody plants. To this end, areas of homogeneous land cover type were identified on the GlobeLand30 map [44]. The GlobeLand30 product [44] is based on 30 m resolution Landsat imagery and classifies land cover types according to the dominant plant life form (e.g. forest, shrubland and grassland), which can be more readily related to distinct fuel types than biome classifications that often include classes of mixed life forms (e.g. woody savanna in MCD12Q1_V51). A large random sample (n = 9,053) of ca. 30 km × 30 km areas of homogeneous land cover type was drawn by sampling 16 blocks of 1000 × 1000, 30 m grid cells from each of the 853 GlobeLand30 tiles and keeping all blocks with at least 75% in a single land cover class. The geographical coordinates of the 9,053 homogeneous sample blocks were first used to extract corresponding values of P and E_0 from the climate grids, which were then used to extract the corresponding domain class from the P, E_0, $F_{0.99}$ response surface.

The distribution of the five global fire regime classes ('pyromes') distinguished by Archibald *et al* [5] over the productivity-limited (PL) and dryness-limited (DL) fire domains was analysed by: (i) mapping all grid cells of the global pyrome map (i.e. figure 2 in 5) to the P, E_0, $F_{0.99}$ response surface via their corresponding mean annual P and E_0, (ii) dividing the global P, E_0 space in 100 mm × 100 mm bins and identifying the pyrome class with the highest relative frequency in all P, E_0 bins with a minimum of 50 data points (n = 185), (iii) a qualitative evaluation of the consistency of the predicted $F_{0.99}$ and relative importance of fuel production and fuel dryness constraints on fire with the defining characteristics of the five pyrome classes [5].

3. Results

3.1. Burned area

The 0.99 quantile of the mean annual fractional burned area, $F_{0.99}$, was found to be a highly predictable function of the climatic water balance terms E and D, and therefore of mean annual precipitation (P) and potential evapotranspiration (E_0) (figures 1(a)–(c)). The means and confidence intervals of the fitted model coefficients are listed in table 1.

Linear regression analysis of observed versus predicted $F_{0.99}$ for validation sites showed that the hydroclimatic model (equation (4), figure 1(c)) explained 80% of the global variation in $F_{0.99}$ ($R^2 = 0.80$), with a

Table 1. Mean and 95% confidence intervals of model coefficients (equation (4)) obtained from 1000 model fits.

Coefficient	Dimension	Mean	95% CIs
E_1	mm.y^{-1}	577	554, 597
E_2	mm.y^{-1}	976	952, 1126
D_1	mm.y^{-1}	607	591, 626
D_2	mm.y^{-1}	1034	986, 1088

Mean Difference (MD) between observed and predicted values of 0.05, Root Mean Squared Deviations (RMSD) of 0.14, Normalised Mean Error (NME) of 0.45 and Normalised Mean Square Error (NMSE) of 0.27. Further details on the validation of the $F_{0.99}$ model are provided in Supplementary Material, S1 (available online at stacks.iop.org/ERC/3/035001/mmedia).

According to the GFED4 data base [2], global burned areas amounted to 2.3% of the terrestrial land area per year over the 1995–2016 observation period. The observed mean annual fractional burned area, F, was highest in the tropical savanna regions of Africa, Australia and (to a lesser extent) South America, where F values in the 0.3–0.4 range were common and as high as 0.7–0.8 in localized areas. In other fire-prone environments, F was much lower, with values of up to ~0.10 for shrublands and in the 0.01–0.03 range for most forests.

The predicted global pattern of $F_{0.99}$ was very similar to the observed pattern of F in the tropical savannas of Sub-Saharan Africa and Australia, where tropical wet-dry climates combine high levels of fuel production during the wet season with intense drought during the dry season, producing F values as high as 0.8–1.0 (figures 2(a)–(b)). In woody ecosystems outside of the tropical savannas and semiarid grasslands $F_{0.99}$ seldom exceeded 0.5, which is consistent with the fact that most predominantly woody vegetation communities cannot survive such high levels of fire activity over long periods [45]. Zonal medians of predicted $F_{0.99}$ were 0.17 for Mediterranean forests, woodlands and scrub, 0.05–0.12 for temperate forests, and 0.01 for boreal forest environments (Supplementary Material, S2).

3.2. Climate-fire domains

The fitted P, E_0, $F_{0.99}$ response surface consists of two distinct domains (figure 1(d)) characterized by different climate constraints on fire [19]. The first domain (green zone in figure 1(d)) is characterized by $F_{0.99}$ increasing with mean annual actual evapotranspiration (E) but not with variation in climatic water deficit (D), consistent with potential fire activity levels being primarily limited by fuel production (hereafter: PL-type fire). In the second domain (orange zone in figure 1(d)), $F_{0.99}$ increases strongly with D but varies little with increasing E, consistent with potential fire activity levels being primarily limited by the capacity of the atmosphere to dry-out fuel material to ignitable levels (DL-type fire).

A visual interpretation of the fitted P, E_0, $F_{0.99}$ response surface suggests that the domain shift from PL-type fire to DL-type fire occurs at some threshold aridity index (i.e. the ratio of mean annual potential evapotranspiration and precipitation: $\frac{E_0}{P}$). The equation for the boundary between the two domains can be derived analytically from equations (1)–(4) and is approximately linear for the region covered by the observations: $E_0 = (1.94 \pm 0.02)P$ ($p < 0.001$ and $R^2 = 0.996$) (Supplementary Material S3). Using gridded mean annual climate data, the domains of PL- and DL-type fire were mapped to geographical space (figure 2(c)). The global pattern of PL- and DL-type fire is similar to the global distribution of climate aridity and biome types, as expected given that the boundary between PL- and DL-type fire corresponds to an aridity index of ~1.9. Dryland environments at mid latitudes on all continents were classified in the domain of PL-type fire, while wet and cold environments at all latitudes were classified in the domain of DL-type fire. The domain classification indicates whether the primary limiting factor on mean annual fire activity levels was fuel production or fuel dryness, which can be expected to correlate strongly with the dominant vegetation lifeform and fuel type (litter versus grass). Using the GLC30 global lifeform mapping [44] we found that areas of forest, wetland and tundra were predominantly classified in the domain of DL-type fire (i.e. they are typically too wet to burn for much of the time), whereas grasslands, shrublands and barren lands were predominantly classified in the domain of PL-type fire (i.e. fuels are typically sparse and discontinuous for much of the time) (figure 3). The shrubland class is an interesting case: these ecosystems occur most frequently in the domain of PL-type fire even though they are dominated by woody vegetation and woody plant litter forms an important fuel component. However, classification as PL-type fire makes sense because (semiarid and arid) shrublands can often only support large fires when herbaceous vegetation fills in the gaps and connects the fuel array after above-average rainfall e.g., [46, 47].

As expected, the five pyromes distinguished by Archibald *et al* [5] were found to occupy distinct domains in P, E_0 climate space (figure 4): (i) the 'RIL' pyrome, characterized by rare, intense, large fires was restricted to low P environments in the climate domain of PL-type fire (green grid cells, figure 4) with a median predicted $F_{0.99}$ of

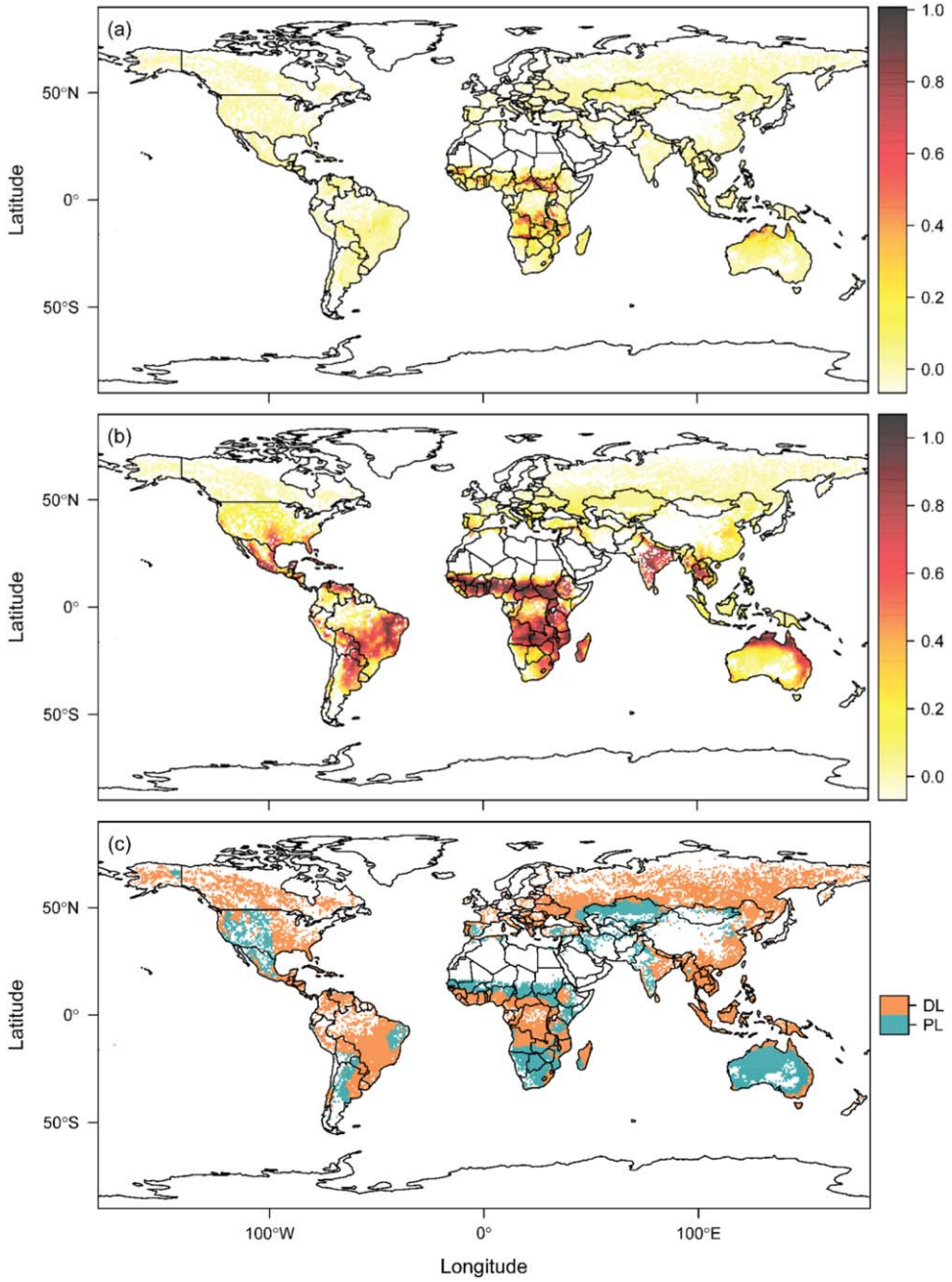

Figure 2. (a) Observed (1995–2016) mean annual fractional burned area (F). (b) Predicted 0.99 quantile of mean annual fractional burned area ($F_{0.99}$). (c) Geographical distribution of domains of PL- and DL-type fire in green and orange tones, respectively. In white land areas the observed mean annual fractional burned area was negligible ($F < 0.000001$).

0.05, consistent with its geographical distribution in the more arid zones of boreal forests and temperate coniferous forests, plus areas of Mediterranean vegetation and xeric vegetation; (ii) the 'FIL' pyrome, characterized by frequent, intense, large fires (yellow grid cells, figure 4), was found in the climate domain of PL-type fire across a broad range of mean annual P combined with high E_0 and with a median predicted $F_{0.99}$ of 0.55, which is typical for the tropical savannas in Australia and Africa where this pyrome prevails; (iii) the 'FCS' pyrome, characterized by frequent, cool (low-intensity), small fires (orange grid cells, figure 4), was found across both climate domains in the region that combines high P, high E_0, and very high predicted $F_{0.99}$ (median = 0.63), corresponding mainly to tropical grasslands and shrublands as well as tropical dry broadleaf forests; iv) the 'RCS' pyrome, characterized by rare, cool, small fires (pink grid cells, figure 4) was found mostly in the domain of DL-type fire in the region of intermediate P and E_0 with the median of predicted $F_{0.99}$ just below 0.09.

The geographical distribution of the RCS pyrome spans all continents and a range of biomes, including large fractions (0.4–0.5) of boreal forests, temperate coniferous and broadleaf forests, as well as smaller fractions (0.2–0.4) of Mediterranean vegetation and Montane grasslands; (v) the 'ICS' pyrome, the most 'human-driven'

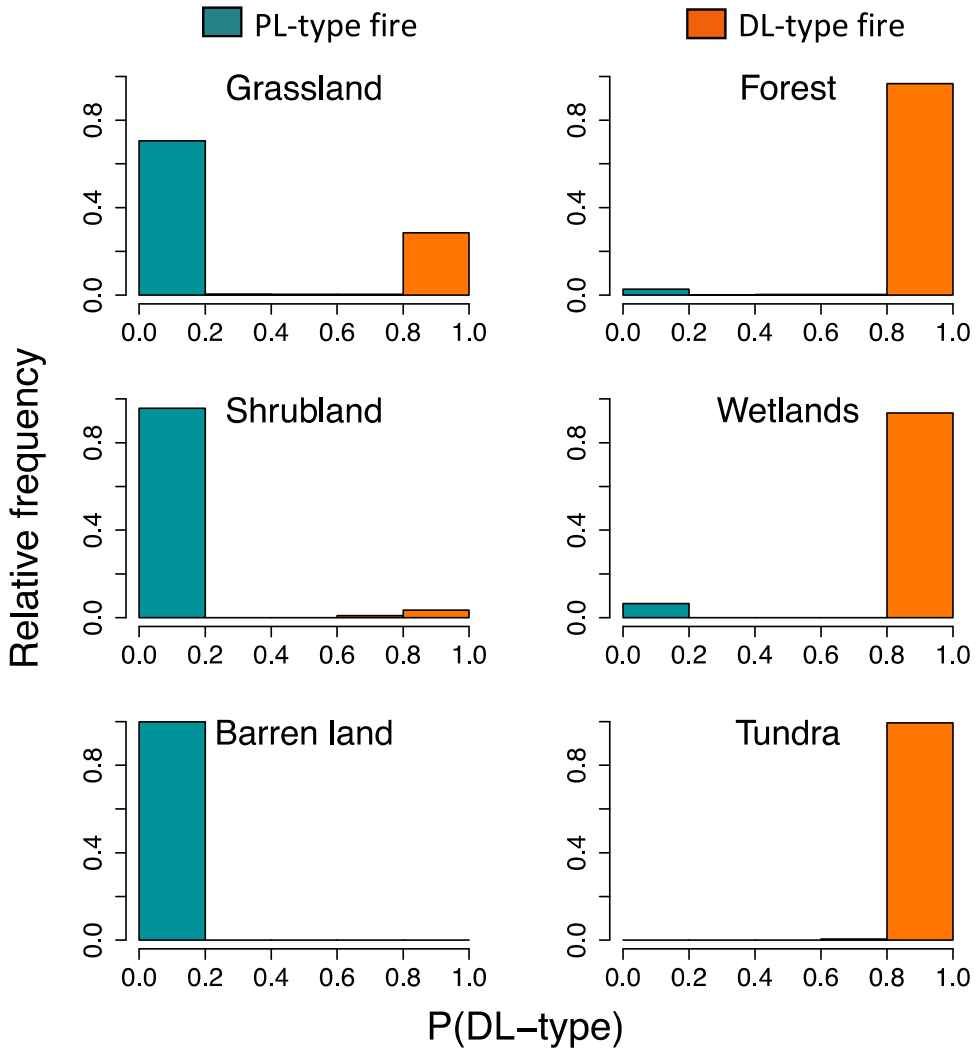

Figure 3. Distributions of probabilities of classification in the domain of DL-type fire for a large sample (n = 9053) of 30 km × 30 km areas of homogenous landcover drawn from the GLC30 global lifeform database [44]. Bars are coloured green where P(DL-type) < 0.5, to indicate prevailing affinity to the domain of PL-type fire, and coloured orange where P(DL-type) > 0.5 to indicate prevailing affinity to the domain of DL-type fire.

pyrome according to Archibald *et al* [5], is characterized by intermediate frequency of cool, small fires (blue grid cells, figure 4) and was found in both climate domains, PL- and DL-type, across wide ranges of P and E_0, which translates to a wide range of predicted $F_{0.99}$ (median = 0.25). The geographical distribution of the ICS pyrome is also widespread, including large fractions (0.4–0.6) of all tropical forest biomes, and smaller but substantial fractions (0.2–0.4) of temperate forests, (tropical) grasslands and shrublands, which is consistent with the spread across climate domains of both fuel productivity limitations (PL-type) and fuel dryness limitations (DL-type).

4. Discussion

This study has shown that climate sets strong and highly predictable constraints on the global distribution of fire on Earth. In particular, climate constrains the amounts and timing of plant available water and energy and thereby determines the probability that the two most basic conditions for fire are met, namely the production and desiccation of plant biomass and derived fuels. We showed that the strength of those two fundamental climate constraints on fire, and global variation therein, are captured well by the mean annual climatic water balance, which provides a simple yet biophysically sound basis for the prediction of potential fractional burned area from just two readily available climate variables: mean annual precipitation and potential evapotranspiration. The proposed hydroclimatic model was validated against independent burned area data and found to explain 80% of the global variation in potential fractional burned area ($F_{0.99}$) with a slight tendency to overpredict $F_{0.99}$, but an NME of 0.45 indicating good agreement between predicted and observed spatial patterns of $F_{0.99}$. A direct comparison of model performance with existing global fire models is difficult since

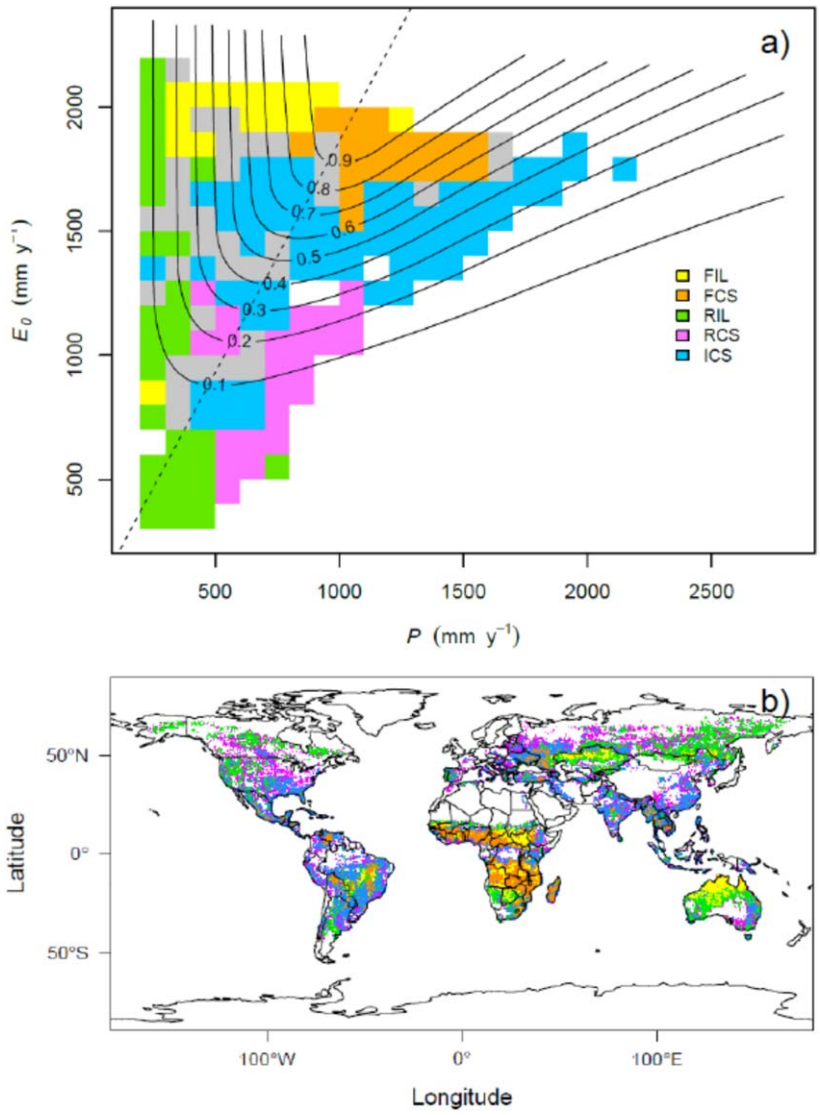

Figure 4. (a) Distribution of global pyrome classes [5] in P, E_0 space, with contours of the fitted global $F_{0.99}$ model in black and grey cells indicating climate space where none of the five pyromes had a relative frequency exceeding 0.2. (b) Geographical distribution of pyrome classes, redrawn from Archibald *et al* [5]. The three-letter pyrome abbreviations refer to the typical fire frequencies, intensities and fire sizes of each pyrome, where FIL is Frequent-Intense-Large, FCS is Frequent-Cool-Small, RIL is Rare-Intense-Large, RCS is Rare-Cool-Small, and ICS is Intermediate-Cool-Small.

most existing models predict F rather than $F_{0.99}$ and systematic evaluation of their performance is ongoing as part of the fire modelling intercomparison project (FIREMIP) [7–10, 48]. Our hydroclimatic model is conceptually similar to a global model proposed by Kelley *et al* [49] that predicts burned area as a function of four limitations (i.e. fuel continuity, fuel moisture, potential ignitions and a suppression index). Kelley *et al* [49] report an NME score of 0.60–0.63 for their model predictions of mean annual burned area against the GFED4s data set [2, 50], indicating a lack of agreement between the spatial pattern of predicted and observed burned area.

Overprediction of $F_{0.99}$ by our model was somewhat more pronounced in environments of the DL-type fire than in environments of PL-type fire (see Supplementary Material, S1), but model residuals had similar distributions for a wide range of MODIS landcover types, supporting the notion that the model captures the main climatic constraints on global fire activity levels. Our model fitting approach, which sought to avoid dominance of the most common fire-prone environments on Earth such as tropical savannas, will have contributed to the relatively good performance of the model across a broad range of hydroclimatic conditions. Existing fire models tend to struggle predicting the fire regimes of temperate and boreal forest regions, that burn much more infrequently than tropical savannas [5], but we did not observe that model fit suffered in any particular biome because we employed a mechanistic, hydroclimatic approach that captured the fundamental biophysics underlying global fire regimes.

The bias in performance of existing global fire models is likely due to a limited capacity to simulate fuel drying dynamics in forest and woodland environments [8, 10]. Whereas the seasonally wet-dry climate of

tropical savannas makes annual production and subsequent desiccation of fuels highly predictable, fire activity in forests and woodlands is primarily constrained by the moisture content of the (inherently abundant) fuels, which varies at (sub)daily to monthly timescales [51–53]. The fuel moisture models within several of the existing global fire models [9] are driven by some implementation of the Nesterov index: $N = \sum_{i=1}^{\omega}(T_i - T_{dp,i})\,T_i$, where ω is the number of days since the last rainfall exceeding 3 mm d^{-1}, T_i is the daily 3 pm air temperature (°C) and $T_{dp,i}$ the daily 3pm dew point temperature (°C). As shown by Schunk *et al* [54] the Nesterov Index was a poor predictor of the moisture content of 1-hour and 10-hour fuels from four main forest species in Germany. With fuel moisture variation modelled by the Nesterov index global fire models lack the critical capacity to predict when, or how frequently, forests and woodlands switch from a moist/non-flammable state to a dry/flammable state and are therefore unlikely to reproduce observed spatiotemporal variation in burned area in those biomes. Substitution of the Nesterov Index with a more reliable (physically-based) fuel moisture model e.g., [55] would likely improve predictions of burned area in forest biomes by those models.

Our hydroclimatic model predicts potential mean annual burned area and does therefore not require predictions of daily fuel moisture content; instead, the mean annual climatic water deficit (D) is used as an estimate of the probability of extant fuels drying out to ignitable levels during some fraction of the year. With D being a measure of the atmospheric moisture demand that cannot be met by the soil water store [18], D captures the basic biophysics involved in the desiccation of fuels and accounts for the fact that sparse fuels (low E) require less energy (E_0) to dry out than dense/heavy fuels.

Further evidence for D being a reasonable indicator of the mean annual probability of forests and woodlands being in a dry fuel state can be derived from previous studies on climate-fire relations in the western United States [22, 23, 25, 56] and studies on dead fuel moisture (Resco de Dios *et al* 2015) and fire activity in temperate forests of SE Australia [51] and Portugal [53] that showed that cumulative burned area in these different forest regions responds strongly non-linearly to predicted fine dead fuel moisture content dropping below thresholds identified at 14%–18% and 10%–12%, respectively. Using the Resco de Dios *et al* [55] fuel moisture model with gridded global vapour pressure deficit data to predict daily fine dead fuel moisture content for global forests and woodlands, we found that mean annual D is strongly and linearly related (adj. R^2: 0.76, $p < 2e\text{-}16$) to the mean annual frequency of predicted daily fine dead fuel moisture content dropping below 10% (Supplementary Material, S4).

The hydroclimatic model allowed us to objectively distinguish climatic domains for a predominance of either fuel productivity (PL-type) or fuel dryness (DL-type) constraints on mean annual fractional burned area, and showed their geographical distribution to be consistent with global patterns of herbaceous versus woody vegetation types and corresponding fuel types, in accordance with the varying constraints hypothesis [21]. Further, we demonstrated (see Supplementary Material, S3) that the boundary between the domains of PL- and DL-type fire is well approximated by an aridity index of 1.9 (1.94 ± 0.02), providing the first objective identification of where in climate space (figure 1(d)), and in geographical space (figure 2(c)), fire regimes switch from fuel load limitations to fuel moisture limitations. We showed that the hydroclimatic model and associated classification in two contrasting climate-fire domains is largely consistent with the hydroclimatic distribution of pyromes [5], indicating that key aspects of global fire regimes vary in a predictable way with global gradients in mean annual precipitation and potential evapotranspiration. This suggests that our model could be used with ensembles of future climate projections to provide insights in the potential for (incremental) changes in mean annual fractional burned area as well as (transformational) changes in the role of fuel production or fuel dryness constraints on fire e.g. [19]

By focusing exclusively on the roles of fuel production and fuel dryness constraints, our hydroclimatic model was designed to predict the potential or maximum mean annual fractional burned area, which provides a useful reference for bottom-up process-based modelling approaches used in many DGVMs [7–9]. Our model could also be used in combination with data-driven approaches to predicting annual, rather than potential mean annual, fractional burned area by modelling the annual deviations between predicted $F_{0.99}$ and observed annual fractional burned area. Recent statistical models of interannual variation in burned area, partly captured climate constraints on fire via fuel production and dryness, but could only explain 30%–40% of the global variation in burned area [25] or showed good agreement between predictions and remotely sensed burned area in only 31%–56% of the global land surface area [10]. Better performance may be achieved by focusing on prediction of annual or monthly deviations from a long-term potential burned area level (e.g. $F_{0.99}$) as a function of annual or seasonal anomalies in climate conditions plus metrics that capture fire weather and ignition constraints on fire activity at shorter time scales, thus completing the formalisation and implementation of the four-switch concept [17]. Other future work could also examine the drivers, such as fire management and other human activities, of geographical variation between F and $F_{0.99}$.

5. Conclusion

At long time scales the global distribution of fire is highly predictable from fundamental biophysical constraints on the production and seasonal desiccation of plant biomass (i.e. fuel), which in turn are proportional to mean annual precipitation and potential evapotranspiration. The sharp transition of global fire regimes from domains of fuel production limitations on fire (PL-type) to fuel dryness limitations on fire (DL-type) can be identified from the mean annual aridity index being above or below a threshold value of ~1.9. Our model provides a simple but comprehensive basis for predicting fire potential under current and future climates, as well as an overarching framework for estimating effects of human activity via ignition regimes and manipulation of vegetation. In these respects, it offers a significant advance on existing global fire models and therefore a basis for improving predictions from coupled global vegetation models.

Acknowledgments

M M B and R A B acknowledge funding support from the New South Wales Department of Planning, Infrastructure and Environment through the NSW Bushfire Risk Management Research Hub. E Z S acknowledges support from the Australian Research Council (DP160103436). We thank Sally Archibald for providing the pyrome classification layer.

Data availability statement

The data that support the findings of this study are openly available at the following URL/DOI:
Global Fire Emissions Database (GFED) data are freely available at: http://www.globalfiredata.org/.
WorldClim gridded climate data can be downloaded from: http://worldclim.org/.
Gridded mean annual global potential evapotranspiration can be downloaded from CGIAR-CSI: https://cgiarcsi.community/data/global-aridity-and-pet-database/.

The Globeland30 (GLC30) global landcover classification layer can be downloaded from: http://www.globallandcover.com/.
The Moderate Resolution Imaging Spectroradiometer (MODIS) landcover classification (MCD12Q1) can be downloaded from: https://lpdaac.usgs.gov/products/mcd12q1v006/
The global pyrome classification layer is available upon request from Sally Archibald.

ORCID iDs

Matthias M Boer https://orcid.org/0000-0001-6362-4572
Víctor Resco De Dios https://orcid.org/0000-0002-5721-1656
Elisa Z Stefaniak https://orcid.org/0000-0003-2998-5619
Ross A Bradstock https://orcid.org/0000-0002-6904-2394

References

[1] Roy D P *et al* 2005 Prototyping a global algorithm for systematic fire-affected area mapping using MODIS time series data *Remote Sens. Environ.* **97** 137–62
[2] Giglio L, Randerson J T and van der Werf G R 2013 Analysis of daily, monthly, and annual burned area using the fourth-generation global fire emissions database (GFED4) *Journal of Geophysical Research: Biogeosciences* **118** 317–28
[3] Robinson J M 1991 Fire from space: global fire evaluation using infrared remote sensing *Int. J. Remote Sens.* **12** 3–24
[4] Chuvieco E and Martin M P 1994 Global fire mapping and fire danger estimation using avhrr images *Photogramm. Eng. Remote Sens.* **60** 563–70
[5] Archibald S *et al* 2013 Defining pyromes and global syndromes of fire regimes *Proc. Natl Acad. Sci.* **110** 6442–7
[6] Gill A M 1975 Fire and the Australia flora: a review *Australian Forestry* **38** 4–25
[7] Hantson S *et al* 2016 The status and challenge of global fire modelling *Biogeosciences* **13** 3359–75
[8] Hantson S *et al* 2020 Quantitative assessment of fire and vegetation properties in simulations with fire-enabled vegetation models from the Fire Model Intercomparison Project *Geosci. Model Dev.* **13** 3299–318
[9] Rabin S S *et al* 2017 The fire modeling intercomparison project (FireMIP), phase 1: experimental and analytical protocols with detailed model descriptions *Geosci. Model Dev.* **10** 175–1197
[10] Forkel M *et al* 2019 Emergent relationships with respect to burned area in global satellite observations and fire-enabled vegetation models *Biogeosciences* **16** 57–76
[11] Knorr W, Arneth A and Jiang L 2016 Demographic controls of future global fire risk *Nat. Clim. Change* **6** 781–5
[12] Archibald S, Staver A C and Levin S A 2012 Evolution of human-driven fire regimes in Africa *Proc. Natl Acad. Sci.* **109** 847–52
[13] Parisien M-A *et al* 2016 The spatially varying influence of humans on fire probability in North America *Environ. Res. Lett.* **11** 075005
[14] Bowman D M J S *et al* 2011 The human dimension of fire regimes on Earth *Journal of Biogeography* **38** 2223–36

[15] Harris R M B *et al* 2016 Climate-vegetation-fire interactions and feedbacks: trivial detail or major barrier to projecting the future of the Earth system? *Wiley Interdisciplinary Reviews-Climate Change* **7** 910–31
[16] Malamud B D, Millington J D A and Perry G L W 2005 Characterizing wildfire regimes in the United States *Proc. Natl. Acad. Sci. USA* **102** 4694–9
[17] Bradstock R A 2010 A biogeographic model of fire regimes in Australia: current and future implications *Global Ecol. Biogeogr.* **19** 145–58
[18] Stephenson N L 1998 Actual evapotranspiration and deficit: biologically meaningful correlates of vegetation distribution across spatial scales *Journal of Biogeography* **25** 855–70
[19] Boer M M *et al* 2016 Future changes in climatic water balance determine potential for transformational shifts in Australian fire regimes *Environ. Res. Lett.* **11** 065002
[20] Cade B S and Noon B R 2003 A gentle introduction to quantile regression for ecologists *Frontiers in Ecology and the Environment* **1** 412–20
[21] Krawchuk M A and Moritz M A 2011 Constraints on global fire activity vary across a resource gradient *Ecology* **92** 121–32
[22] McKenzie D and Littell J S 2017 Climate change and the eco-hydrology of fire: Will area burned increase in a warming western USA? *Ecological Applications* **27** 26–36
[23] Littell J S and Gwozdz R B 2011 Climatic water balance and regional fire years in the pacific Northwest, USA: linking regional climate and fire at landscape scales *The Landscape Ecology of Fire* ed D McKenzie *et al* (Netherlands: Dordrecht: Springer) pp 117–39
[24] Bailey R G 1995 *Description of the ecoregions of the United States, in Miscellaneous Publication 1391 (revised).* (Washington: U.S. Forest Service)
[25] Abatzoglou J T *et al* 2018 Global patterns of interannual climate–fire relationships *Global Change Biol.* **24** 5164–75
[26] Rosenzweig M L 1968 Net primary productivity of terrestrial communities: prediction from climatological data *The American Naturalist* **102** 67–74
[27] Yang Y, Long D and Shang S 2013 Remote estimation of terrestrial evapotranspiration without using meteorological data *Geophys. Res. Lett.* **40** 3026–30
[28] Meentemeyer V, Box E O and Thompson R 1982 World patterns and amounts of terrestrial plant litter production *BioScience* **32** 125–8
[29] Matthews E 1997 Global litter production, pools, and turnover times: estimates from measurement data and regression models *Journal of Geophysical Research: Atmospheres* **102** 18771–800
[30] Budyko M I 1958 *The Heat Balance of the Earth's Surface.* (Washington, D.C.: The US Dept. of Commerce.) 259
[31] Zhang Y *et al* 2010 Using long-term water balances to parameterize surface conductances and calculate evaporation at 0.05 degrees spatial resolution *Water Resour. Res.* **46** W05512
[32] Williams C A *et al* 2012 Climate and vegetation controls on the surface water balance: synthesis of evapotranspiration measured across a global network of flux towers *Water Resour. Res.* **48** W06523
[33] Wang C *et al* 2016 Advances in hydrological modelling with the Budyko framework: a review *Progress in Physical Geography: Earth and Environment* **40** 409–30
[34] Murphy B P *et al* 2013 Fire regimes of Australia: a pyrogeographic model system *Journal of Biogeography* **40** 1048–58
[35] Yin X *et al* 2003 A flexible sigmoid function of determinate growth *Annals of Botany* **91** 361–71
[36] Hijmans R J *et al* 2005 Very high resolution interpolated climate surfaces for global land areas *Int. J. Climatol.* **25** 1965–78
[37] Zomer R J *et al* 2007 *Trees and Water: Smallholder Agroforestry on Irrigated Lands in Northern India.* (Colombo, Shri Lanka: International Water Management Institute) p 45 IWMI Research Report 22
[38] Zomer R J *et al* 2008 Climate change mitigation: a spatial analysis of global land suitability for clean development mechanism afforestation and reforestation *Agriculture, Ecosystems & Environment* **126** 67–80
[39] R Core Team, R 2019 *A Language and Environment for Statistical Computing.* (Vienna, Austria: R Foundation for Statistical Computing)
[40] Hijmans R J *et al* 2019 raster: Geographic Data Analysis and Modeling. R package version 3.0-7. (https://rspatial.org/raster)
[41] Koenker R 2017 quantreg: Quantile Regression. R package version 5.33. (https://www.r-project.org)
[42] Geyer C J 2011 *Introduction to MCMC, in Handbook of Markov Chain Monte Carlo* ed S P Brooks *et al* (Boca Raton, FL: Chapman & Hall/CRC) pp 3–48
[43] Kelley D I *et al* 2013 A comprehensive benchmarking system for evaluating global vegetation models *Biogeosciences* **10** 3313–40
[44] Chen J *et al* 2015 Global land cover mapping at 30 m resolution: A POK-based operational approach *ISPRS J. Photogramm. Remote Sens.* **103** 7–27
[45] Bond W J and Keeley J E 2005 Fire as a global 'herbivore': the ecology and evolution of flammable ecosystems *Trends Ecol. Evol.* **20** 387–94
[46] O'Donnell A J *et al* 2011 Climatic anomalies drive wildfire occurrence and extent in semi-arid shrublands and woodlands of southwest Australia *Ecosphere* **2** art127
[47] Prior L D *et al* 2017 Does inherent flammability of grass and litter fuels contribute to continental patterns of landscape fire activity? *Journal of Biogeography* **44** 1225–38
[48] Teckentrup L *et al* 2019 Sensitivity of simulated historical burned area to environmental andanthropogenic controls: A comparison of seven fire models *Biogeosciences Discuss.* **2019** 1–39
[49] Kelley D I *et al* 2019 How contemporary bioclimatic and human controls change global fire regimes *Nat. Clim. Change* (https://doi.org/10.1038/s41558-019-0540-7)
[50] Randerson J T *et al* 2012 Global burned area and biomass burning emissions from small fires *Journal of Geophysical Research-Biogeosciences* **117** G04012
[51] Nolan R H *et al* 2016 Large-scale, dynamic transformations in fuel moisture drive wildfire activity across southeastern Australia *Geophys. Res. Lett.* **43** 4229–38
[52] Caccamo G *et al* 2012 Using remotely-sensed fuel connectivity patterns as a tool for fire danger monitoring *Geophys. Res. Lett.* **39** L01302
[53] Boer M M *et al* 2017 Changing Weather extremes call for early warning of potential for catastrophic fire *Earth's Future* **5** 1196–202
[54] Schunk C *et al* 2017 Fine fuel moisture for site- and species-specific fire danger assessment in comparison to fire danger indices *Agric. For. Meteorol.* **234–235** 31–47
[55] Resco de Dios V *et al* 2015 A semi-mechanistic model for predicting the moisture content of fine litter *Agric. For. Meteorol.* **203** 64–73
[56] Williams A P *et al* 2015 Correlations between components of the water balance and burned area reveal new insights for predicting forest fire area in the southwest United States *International Journal of Wildland Fire* **24** 14–26